IEEE Access
Multidisciplinary | Rapid Review | Open Access Journal

Received December 16, 2017, accepted February 11, 2018, date of publication March 19, 2018, date of current version April 4, 2018.

*Digital Object Identifier 10.1109/ACCESS.2018.2812890*

# Denoised Maximum Likelihood Estimation of Chest Wall Displacement from the IR-UWB Spectrum

**VAN NGUYEN[1] AND MARY ANN WEITNAUER[2], (Senior Member, IEEE)**
[1]Qualcomm Technologies, Inc., San Diego, CA 92121, USA
[2]School of Electrical and Computer Engineering, Georgia Institute of Technology, Atlanta, GA 30332, USA
Corresponding author: Van Nguyen (vannguyen@gatech.edu)

**ABSTRACT** We present a novel method of estimating the chest wall displacement *in the frequency domain* from a narrow portion of the IR-UWB radar received spectrum. A Maximum Likelihood (ML) estimator of the displacement is designed, and the associated bias and Cramér-Rao lower bound of the ML estimator are analyzed. To improve estimation accuracy, empirical mode decomposition is applied to denoise the ML-estimated displacement. Simulation studies are conducted to evaluate the performance of the proposed method under realistic system parameter values. The computational complexity of the proposed method is low and equal to that of the Discrete Fourier Transform.

**INDEX TERMS** Bias, Cramér-Rao lower bounds, denoising, displacement estimation, IR-UWB radar, maximum likelihood estimator.

## I. INTRODUCTION

Chest displacement has clinical significance in identifying cardiopulmonary disorders. Chest displacement recorded during sleep is a part of the polysomnogram (PSG), the gold standard diagnostic tool in sleep medicine, and is valuable in diagnosis of sleep disorders such as sleep apnea [1], [2]. During unobstructed respiration, a linear relationship between tidal volume and chest wall displacement have been shown in a number of studies [3]–[5]. In addition, the complex intrathoracic motion of the heart also causes minute displacement of the chest wall, which if measurable could be useful in diagnosis of cardiac disorders.

Many methods have been proposed to reconstruct chest wall displacement. The most common tool is inductance plethysmography, in which an adhesive elastic band(s) is applied on the chest wall or abdomen surface. While being low cost and simple, there are several concerns about this method. Its sensitivity is strongly dependent on the tightness of the elastic band [6]. In addition, the band does not provide absolute chest wall displacement directly, rather it measures the relative change in the ribcage circumference [4]. Also, attaching sensors to the body can be restrictive, can disrupt sleep, and can cause discomfort, distress, or pain especially for long-term monitoring. Furthermore, some patients, such as burned patients or those with skin ulcers, cannot accept skin attachments. Several other methods reconstruct heartbeat-induced displacement during absence of breathing based on capacitance variation [7] or electromagnetic field interaction [8] between a sensing probe and the moving chest surface, but are limited by skin attachment or low reproducibility, unstableness, and low rate of obtaining recordings of adequate quality for data analysis [9].

Problems associated with skin attachment can be avoided with non-contact methods. Laser techniques have been proposed for displacement sensing of generic target surface [10] and chest wall in particular [4], [11]–[14]. However, laser sensors do not offer through-clothes sensing, causing inconvenience and unsuitability for continuous monitoring.

Continuous wave (CW) Doppler radar can penetrate through clothes, and has been proposed for non-contact chest wall displacement sensing in many studies [6], [15]–[19]. These methods typically perform DC offset calibration to estimate the undesired DC offsets present in the two quadrature baseband signal channels, followed by arctangent demodulation [16] to obtain displacement information. Wavelet filtering and ensemble empirical mode decomposition [20] have also been added to improve estimation accuracy [18]. Good agreement with gold standard method such as overnight PSG recordings has been demonstrated [6]. However, these methods face several challenges. Existing DC

offset calibration methods have been shown to be strongly dependent on one or a combination of factors such as displacement amplitude, displacement morphology, and noise levels [6], [21], [22]. Examples include erroneous or arbitrary DC offsets estimation result for small breathing displacement amplitude or when the constellation diagram of the in-phase and quadrature baseband channels is not close enough to an arc shape [6]. In addition, phase imbalance and amplitude imbalance between the two channels can cause errors in the arctangent estimator of the displacement [15].

While many studies exist for applying Doppler radar on *non-contact* chest wall displacement estimation, few exist for IR-UWB radar. The major advantage of IR-UWB in this application is IR-UWB's benign co-existence properties. To qualify to be UWB, the signal must have a 10-dB bandwidth that is at least 20% of the center frequency or at least 500 MHz [23]. Because of its extremely low spectral power density - orders of magnitude lower than mobile communication signals - it makes negligible interference on other wireless systems in its band (3 GHz-10 GHz) and their interference has negligible effect on the UWB receiver [24]. The IR-UWB radar transmits a series of extremely narrow (on the order of sub-nanosecond wide) pulses to the chest, and the pulses reflect off the chest and arrive at the receive antenna. The round trip propagation delay is directly related to the distance between the chest and the radar system. The novelty of this paper is a Denoised Maximum Likelihood (DML) estimator of an arbitrary chest displacement waveform from only a narrow portion of the IR-UWB radar received spectrum. In-depth analysis of the bias and CRLB will also be presented.

For IR-UWB radar, some existing methods perform direct sampling of the backscattered RF waveforms, and then either detect the waveform peaks [25], [26] or compute the correlation with a reference waveform [27], [28] to obtain the absolute or relative pulse delays, which are associated with the chest displacement. However, these methods require extremely high sampling rate (tens of GHz). Specialized radar system designs have been proposed [29]–[33], where cross correlation is obtained by hardware, transforming the received RF pulses into a low-frequency equivalent which can be digitized at a much lower sampling rate. Muragaki and coworkers [34] perform chest displacement estimation with UWB radar based on the direct phase demodulation proposed for CW Doppler radar, however the residual phase noise inherent in this method is not addressed. Sana and coworkers [35] propose a respiratory movement estimation scheme based on time-domain subsampling and sparse vector estimation of the channel impulse response using a Bayesian framework. However, the method assumes that the received signals at each pulse interval in the observation window have identical round-trip delays. In our proposed method, we do not impose this assumption.

Unlike the related works mentioned above, which are time domain approaches, an iterative time-delay estimation algorithm based on the weighted Fourier transform has been proposed in [36]. In this study, the received signal comprises copies of a known signal with different amplitudes and delays. The delays are estimated from the received signal spectrum using an iterative algorithm. Each step comprises one or more one-dimensional search procedures that use the Fast Fourier Transform (FFT) followed by a fine search algorithm. The number of such search procedures grows quadratically with the number of copies, or equivalently, the number of time delays to be estimated. Another limitation is possible convergence to local minima. In addition, since this algorithm requires direct sampling of the backscattered signal, extremely high sampling rate is needed if applied to IR-UWB pulse delay estimation, as demonstrated in the work itself as well as mentioned earlier for [25]–[28]. Potential application of periodic breathing pattern estimation from the IR-UWB complex spectral amplitudes has been suggested in another study [37].

In this paper, we propose a novel low-complexity chest displacement estimator in the *frequency domain*. A striking feature that differs from existing methods is that only a narrow portion of the UWB received spectrum is needed to reconstruct the entire chest displacement waveform with a computational complexity as low as that of the Discrete Fourier Transform (DFT). The estimator is based on the maximum likelihood principle, and the associated bias and Cramér-Rao lower bound (CRLB) are analyzed. Theoretical limits for estimators developed with UWB radar signal have been either derived or formulated. Zhang *et al.* [38] analyzes CRLBs for pulse delay estimation for UWB synchronization, but the pulses within an observation window are assumed to have the same roundtrip delay. This assumption is not valid for a moving reflecting interface, such as the chest surface. Assuming the chest displaces according to a periodic waveform, Gezici [39] formulated the CRLBs of the waveform parameters. A Maximum Likelihood (ML) estimator that requires an exhaustive search over a multi-dimensional parameter space is formulated, and an efficient sub-optimal solution based on matched filtering and least squares fitting is proposed. However, both the CRLBs and estimators are based on the assumption that the chest displaces according to some known parametric, periodic, analytical function. In reality, the chest displacement can follow an unknown irregular pattern such as during obstructed breathing, and is typically non-stationary even during normal breathing [40]. In addition, the ML estimator complexity in [39] can be prohibitive for real-time applications due to the exhaustive search. In contrast, our ML estimator directly estimates an *arbitrary* chest displacement waveform with conceptually and computationally simple closed-form expressions.

In order to improve estimation accuracy, especially under low SNR, a denoising method is applied to our ML estimates. In this paper, Empirical Mode Decomposition (EMD) [41] is chosen as the denoising technique, but other denoising techniques such as Independent Component Analysis (ICA) [42] can also be used.

Since only a narrow portion of the UWB bandwidth is needed, the proposed method offers significant sampling rate reduction over the conventional digital correlation technique via passband sampling [43]. Computational complexity of the ML estimator is on the order of the DFT. When followed with denoising, the complexity is on the order of the DFT or the denoising method, whichever is larger. As shown in [44], the complexity of EMD is the same with that of an FFT, thus the Denoised ML estimator (ML estimator followed by denoising, or DML) with EMD has complexity of the DFT.[1] Thus, our proposed method is practical for real-time applications.

Although chest displacement estimation is the focused application of this paper, the presented method could also be applied in remote monitoring of displacement of other targets such as civil structures. Structural displacement monitoring applications have been suggested for CW Doppler radar [21] and vision-based sensors [45].

The paper is organized as follows. Section II describes the estimation methods. Section III presents the bias and CRLB analysis. Section IV shows simulation results. Discussion and conclusion are given in Sections V and VI, respectively.

## II. METHODS

In this section, derivation of the proposed estimator will be presented. The noiseless baseband IR-UWB radar received signal can be expressed as

$$s(t) = \sum_{n=0}^{N-1} p_0\left(t - nT_r - \frac{2D_0}{c} - \Delta_n\right), \tag{1}$$

where $N$ is the number of pulses received, $p_0(t)$ is the transmitted UWB pulse shape, $T_r$ is the pulse repetition period, $D_0$ is the nominal distance between the radar and the chest, $c = 3 \times 10^8$ m/s is the pulse propagation speed, $\Delta_n$ is the additional delay that the moving chest wall imposes on the $n^{th}$ pulse.

Let $p(t) = p_0\left(t - \frac{2D_0}{c}\right)$. Then (1) becomes

$$s(t) = \sum_{n=0}^{N-1} p(t - nT_r - \Delta_n). \tag{2}$$

The Continuous Time Fourier Transform of this is

$$\begin{aligned} S(f) &= P(f) \sum_{n=0}^{N-1} e^{-j2\pi f(nT_r + \Delta_n)} \\ &= P(f) \sum_{n=0}^{N-1} e^{-j2\pi f \Delta_n} e^{-j2\pi f n T_r}. \end{aligned} \tag{3}$$

Denote $f_r = 1/T_r$ as the pulse repetition frequency. Evaluating (3) in the neighborhood of the $M^{th}$ pulse repetition frequency harmonic, $f = Mf_r + kf_r/N$, for $k \in [0, N-1]$,

[1] A procedure that performs several sequential tasks, each of which has complexity of $\mathcal{O}(K)$, also has complexity of $\mathcal{O}(K)$

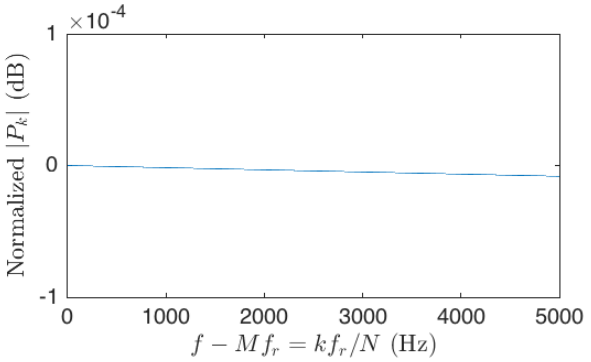


**FIGURE 1.** Samples $P[k]$'s of a UWB pulse being a $7^{th}$-order Gausisian monocycle with bandwidth scaling factor of 0.3 ns [46].

and after some manipulation, we obtain

$$\begin{aligned} S\left(Mf_r + \frac{kf_r}{N}\right) = P\left(Mf_r + \frac{kf_r}{N}\right) \\ \times \sum_{n=0}^{N-1} e^{-j2\pi(Mf_r + \frac{kf_r}{N})\Delta_n} e^{-j\frac{2\pi kn}{N}}. \end{aligned} \tag{4}$$

For the remaining of this paper, $Mf_r$ is regarded to be in the GHz range, which is consistent with the UWB frequency band. Criteria to determine $M$ will be given in Section III-D. In this case, $\frac{kf_r}{N} < f_r \ll Mf_r$, since $f_r$ is typically on the order of kHz in practical IR-UWR radar systems. Consequently, the $\frac{kf_r}{N}$ term in the first exponential term of (4) can be dropped. Denote $P[k] = P(Mf_r + \frac{kf_r}{N})$ and $x[n] = e^{-j2\pi Mf_r \Delta_n}$. A plot of $|P[k]|$ for $f_r = 5$ kHz, $M = 1,063,846$ (so $Mf_r \approx 5.32$ GHz), and $N = 65,536$ is depicted in Fig. 1, showing $P[k]$ is nearly a constant as a function of $k$.

Thus, (4) becomes

$$S\left(Mf_r + \frac{kf_r}{N}\right) \approx P[k] \sum_{n=0}^{N-1} x[n] e^{-j\frac{2\pi kn}{N}} = P[k]X[k], \tag{5}$$

where $X[k]$ is the $N$-point DFT of the discrete time sequence $x[n], n = 0, \ldots, N-1$.

Let $z_k$ be the received signal spectrum at the frequency $f = Mf_r + \frac{kf_r}{N}$, for $k = 0, 1, \ldots, N-1$. Then,

$$z_k = P[k]X[k] + v_k, \tag{6}$$

where $\{v_k\}$ is an additive noise modeled as i.i.d. zero mean complex Gaussian random variables with variance $N_0$.

Denote $P_k = P[k]$ and $X_k = X[k]$. Then (6) is rewritten as

$$z_k = P_k X_k + v_k. \tag{7}$$

Denote

$$Y_k = z_k/P_k = X_k + v_k/P_k. \tag{8}$$

An example plot of $Y_k$'s is shown in Fig. 2. Fig. 2a depicts the entire frequency range of $kf_r/N$ for $k = 0, 1, \ldots, N-1$. Here $f_r = 5$ kHz, $Mf_r \approx 5.32$ GHz, so the range of frequency is the narrow band from 5.32 to 5.325 GHz, with SNR = 6 dB. It is observed that the majority of the spectrum

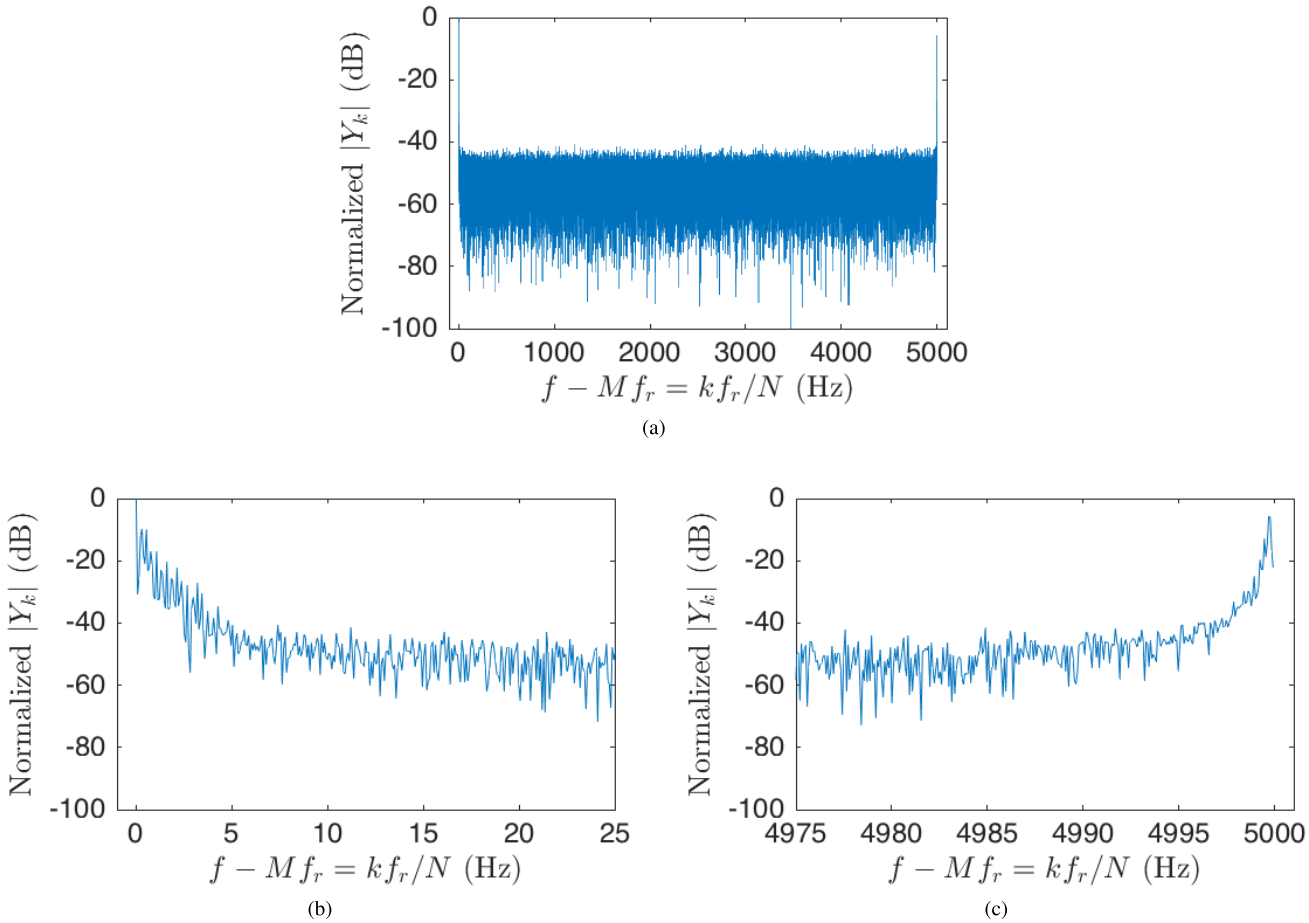


**FIGURE 2.** Plots of (a) $Y_k$'s over the entire frequency band of $f_r = 5$ kHz starting from $Mf_r \approx 5.32$ GHz, and the close-up version of the (b) first and (c) last 25 Hz of the frequency band. SNR = 6 dB.

energy concentrates near the range edges. The spectrum corresponding to the first and last 25 Hz of the range is replotted in Fig. 2b and 2c, respectively.

Taking the IDFT of $Y_k$ ((8)) yields

$$\begin{aligned} y_n &= IDFT_N(Y_k) \\ &= x_n + w_n \end{aligned} \tag{9}$$

where $w_n = IDFT(v_k/P_k) \sim \mathcal{CN}(0, \sigma_w^2)$, with $\sigma_w^2 = N_0/(N|P_0|^2)$, since $\{v_k/P_k\}$ is a zero mean, white complex Gaussian random process with variance $N_0/|P_k|^2 \approx N_0/|P_0|^2$.

Denote

$$\theta_n = -2\pi M f_r \Delta_n \tag{10}$$

Then (9) becomes

$$y_n = e^{j\theta_n} + w_n \tag{11}$$

The following vector notation will be used:

$$\begin{aligned} \boldsymbol{\theta} &= [\theta_0, \theta_1, \ldots, \theta_{N-1}]^T \\ \mathbf{y} &= [y_0, y_1, \ldots, y_{N-1}]^T \\ \mathbf{w} &= [w_0, w_1, \ldots, w_{N-1}]^T \end{aligned}$$

Based on (11),

$$\mathbf{y} = \exp(j\boldsymbol{\theta}) + \mathbf{w}.$$

where $\mathbf{w} \sim \mathcal{CN}(0, \sigma_w^2\mathbf{I})$.

The likelihood of $\theta$ corresponding to the measurement vector $\mathbf{y}$ is

$$\begin{aligned} p(\mathbf{y}|\theta) &= \frac{1}{(\pi\sigma_w^2)^N} \exp\left\{-\frac{1}{\sigma_w^2}\,||\mathbf{y} - \exp(j\boldsymbol{\theta})||_2^2\right\} \\ &= \frac{1}{(\pi\sigma_w^2)^N} \exp\left\{-\frac{1}{\sigma_w^2}\sum_{n=0}^{N-1}\left|y_n - e^{j\theta_n}\right|^2\right\} \end{aligned}$$

The log likelihood is

$$\ln p(\mathbf{y}|\theta) = -N\ln(\pi\sigma_w^2) - \frac{1}{\sigma_w^2}\sum_{n=0}^{N-1}\left|y_n - e^{j\theta_n}\right|^2$$

After rather tedious manipulation, the partial derivatives of the log likelihood are derived as

$$\frac{\partial}{\partial\theta_m}\ln p(\mathbf{y}|\theta) = \frac{2}{\sigma_w^2} r_m \sin(\phi_m - \theta_m),$$

where $y_m = r_m e^{j\phi_m}$, $m = 0, 1, \ldots, N-1$.

Therefore, the ML estimate of the phase vector $\theta$ is

$$\hat{\boldsymbol{\theta}} = \boldsymbol{\phi}$$

where $\boldsymbol{\phi} = [\phi_0, \phi_1, \ldots, \phi_{N-1}]^T$

Let $\Delta = [\Delta_0, \Delta_1, \ldots, \Delta_{N-1}]^T$ be the pulse delay vector. Its ML estimate is

$$\hat{\Delta} = -\frac{1}{2\pi M f_r}\boldsymbol{\phi}$$

Let $d_n = c\Delta_n/2$ be the chest displacement corresponding to the $n^{th}$ pulse, and $\mathbf{d} = [d_0, d_1, \ldots, d_{N-1}]^T$. The ML displacement estimate is

$$\hat{\mathbf{d}} = -\frac{c}{4\pi M f_r}\boldsymbol{\phi}$$

Although the sequence of ML displacement estimates follows the waveform of the chest displacement, as will be shown in Section IV, it is noisy. In order to reduce noise from the estimates, a denoising method is applied. Examples of denoising methods include EMD [41] and ICA [42]. In this paper, EMD is selected as the denoising method. The ML estimator followed by denoising will be referred to as the denoised ML estimator, or DML estimator.

## III. BIAS AND CRAMÉR-RAO LOWER BOUND OF THE MAXIMUM-LIKELIHOOD CHEST DISPLACEMENT ESTIMATOR

In this section, bias and CRLB are analyzed, and the criteria for selecting the frequency portion of the received spectrum used for estimation are specified.

### A. FISHER INFORMATION MATRIX (FIM)

The $mn^{th}$ element of the FIM is $F_{mn} = E\left[-\frac{\partial^2 \ln p(\mathbf{y}|\boldsymbol{\theta})}{\partial\theta_m \partial\theta_n}\right]$ and can be derived or found directly in [47]

$$F_{ml} = \frac{2}{\sigma_w^2}\sum_{n=0}^{N-1}\frac{\partial\mu_n}{\partial\theta_m}\frac{\partial\mu_n}{\partial\theta_l} + \frac{\partial\nu_n}{\partial\theta_m}\frac{\partial\nu_n}{\partial\theta_l}$$

where $\mu_n = \cos(\theta_n)$ and $\nu_n = \sin(\theta_n)$. It can be easily shown that

$$\mathbf{F} = \frac{2}{\sigma_w^2}\mathbf{I}. \tag{12}$$

### B. BIAS

$$E[\hat{\boldsymbol{\theta}}] = E[\boldsymbol{\phi}] = [E[\phi_0], E[\phi_1], \ldots, E[\phi_{N-1}]]^T \tag{13}$$

$$E[\hat{\theta}_n] = \int_{-\pi}^{\pi}\phi_n p(\phi_n|\theta)d\phi_n = \int_{-\pi}^{\pi}\phi_n p(\phi_n|\theta_n)d\phi_n \tag{14}$$

where the conditional density is obtained based on the general result in [48]

$$p(\phi_n|\theta_n) = \frac{1}{2\pi}e^{-\frac{1}{\sigma_w^2}}\left[1 - \sqrt{\pi}\alpha_n e^{\alpha_n^2}\text{erfc}(\alpha_n)\right],$$

where $\alpha_n = -\sqrt{\frac{1}{\sigma_w^2}}\cos(\phi_n - \theta_n)$ and erfc(.) is the complementary error function defined as $\text{erfc}(u) = \frac{2}{\sqrt{\pi}}\int_u^\infty e^{-t^2}dt$. Fig. 3 plots $p(\phi_n|\theta_n)$ for various values of $\theta_n$ for $\sigma_w^2 = 10$. Fig. 4 plots $p(\phi_n|\theta_n)$ for $\theta_n = -0.4\pi$ and various values of $\sigma_w^2$.

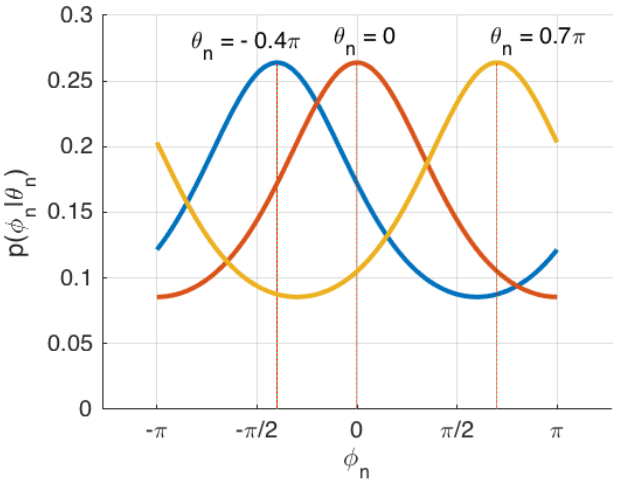


**FIGURE 3.** Plots of $p(\phi_n|\theta_n)$ for various values of $\theta_n$ and $\sigma_w^2 = 10$.

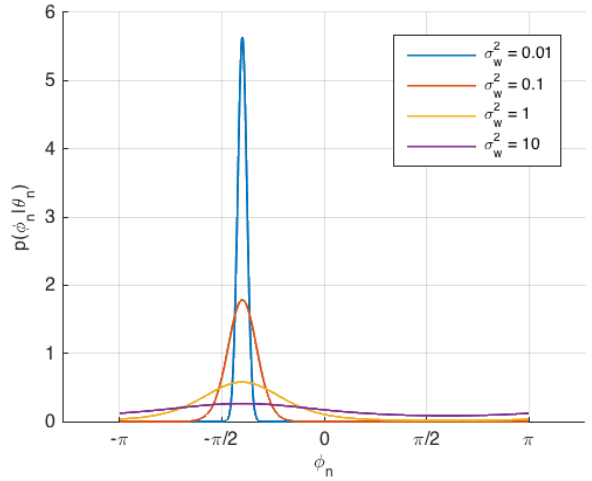


**FIGURE 4.** Plots of $p(\phi_n|\theta_n)$ for $\theta_n = -0.4\pi$ and various values of $\sigma_w^2$.

The bias of the estimator $\hat{\theta}_n$ is defined as

$$b(\theta_n) = E(\hat{\theta}_n) - \theta_n$$

and is depicted in Fig. 5. It is observed that $\hat{\theta}_n$ is a biased estimator. The bias increases quickly near the edges and reaches extreme values at $\pm\pi$. The bias approaches zero when $\sigma_w^2 \to 0$ and approaches the line $b(\theta_n) = -\theta_n$ as $\sigma_w^2 \to \infty$.

The vector of the bias of all parameters in $\theta$ is defined as

$$\mathbf{b}(\boldsymbol{\theta}) = [b(\theta_0), b(\theta_1), \ldots, b(\theta_{N-1})]^T$$

### C. CRAMÉR-RAO LOWER BOUND

Let $\boldsymbol{\epsilon} = \hat{\boldsymbol{\theta}} - \boldsymbol{\theta}$. Since $\hat{\boldsymbol{\theta}}$ is a biased estimator, the CRLB on the mean squared error matrix is expressed as [49]

$$E[\boldsymbol{\epsilon}\boldsymbol{\epsilon}^T] \geq \mathbf{b}(\boldsymbol{\theta})\mathbf{b}^T(\boldsymbol{\theta}) + (\mathbf{I} + \nabla_{\boldsymbol{\theta}}\mathbf{b})\mathbf{F}^{-1}(\mathbf{I} + \nabla_{\boldsymbol{\theta}}\mathbf{b})^T \tag{15}$$

where $\nabla_\theta\mathbf{b}$ is the gradient matrix with elements of the form

$$[\nabla_\theta\mathbf{b}]_{mn} = \frac{\partial b_m}{\partial\theta_n}.$$

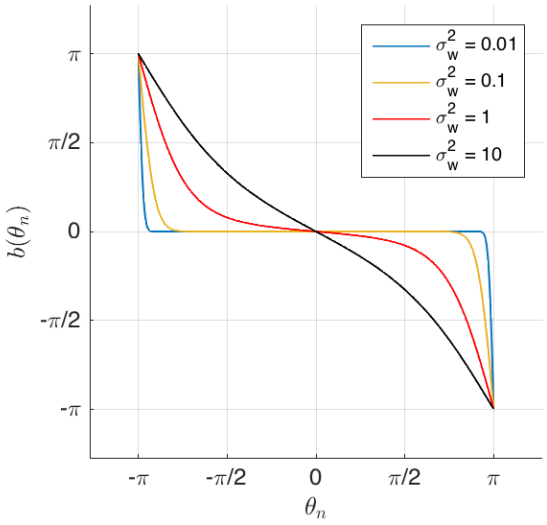


**FIGURE 5.** Bias of $\hat{\theta}_n$.

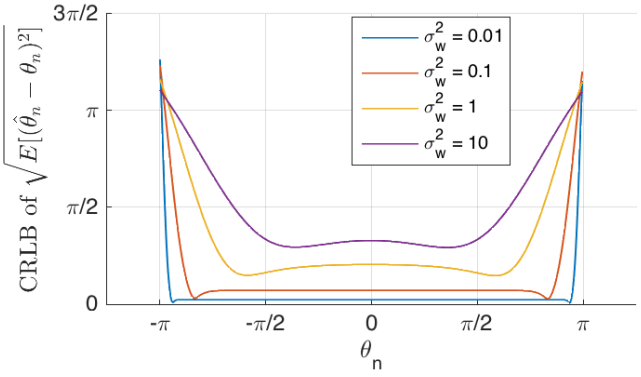


**FIGURE 6.** CRLB of the root mean squared estimation error of $\theta_n$. Note that the presented CRLB is associated with the ML estimator $\hat{\theta}_n$. Only in the case of unbiased estimators is the CRLB independent of the estimator used [49].

A matrix is lower-bounded by a second matrix if the difference between the two is a positive semidefinite matrix.

It follows that the mean squared errors of $\hat{\theta}_n$'s are bounded by the diagonal elements of the right-hand side of (15)

$$E[(\hat{\theta}_n - \theta_n)^2] \geq b^2(\theta_n) + [(\mathbf{I} + \nabla_{\boldsymbol{\theta}}\mathbf{b})\mathbf{F}^{-1}(\mathbf{I} + \nabla_{\boldsymbol{\theta}}\mathbf{b})^T]_{nn}$$

Fig. 6 shows the CRLB of the root mean squared error of $\hat{\theta}_n$.

Then the MSE of the chest displacement estimator is related to that of the phase estimator by

$$E[(\hat{\mathbf{d}} - \mathbf{d})(\hat{\mathbf{d}} - \mathbf{d})^T] = \left(\frac{c}{4\pi Mf_r}\right)^2 E[\boldsymbol{\epsilon}\boldsymbol{\epsilon}^T], \tag{16}$$

where $c$ is the propagation speed of a pulse.

It follows that the CRLB of the $d_n$ estimate is

$$E[(\hat{d}_n - d_n)^2] \geq \left(\frac{c}{4\pi Mf_r}\right)^2 \times \left\{b^2(\theta_n) + [(\mathbf{I} + \nabla_{\boldsymbol{\theta}}\mathbf{b})\mathbf{F}^{-1}(\mathbf{I} + \nabla_{\boldsymbol{\theta}}\mathbf{b})^T]_{nn}\right\}. \tag{17}$$

The CRLB is a function of the parameters to be estimated. Estimate of each displacement sample has a lower bound as shown in (17). The mean squared error defined for the entire sequence of $N$ displacement samples is expressed as

$$E\left[\frac{1}{N}\sum_{n=0}^{N-1}(\hat{d}_n - d_n)^2\right] \geq \frac{1}{N}\sum_{n=0}^{N-1} B_n, \tag{18}$$

where $B_n$ is the right-hand side of (17), i.e., the CRLB of the estimate of $d_n$.

The sequence MSE is lower-bounded by the average of the individual CRLBs. The RMSE and its CRLB is defined by taking the square root of the left-hand side and right-hand side of (18), respectively.

### D. SELECTION OF M

As seen in (17), the CRLB of the displacement pattern is inversely proportional to the square of $Mf_r$, so $Mf_r$ should be large. However, it is also proportional to the CRLB of $\theta_n$. Based on Fig. 6, the CRLB of $\theta_n$ is low for small $|\theta_n|$, notably for $|\theta_n| \leq \pi/2$. Thus, $Mf_r$ should therefore be upper-bounded, based on (10). In addition, $|P(Mf_r)|$ should be large since it is desired that $\sigma_w^2$, which controls how much $\phi_n$ deviates from $\theta_n$, is small.

In summary, the cluster index $M$ is selected *a-priori* to have the following properties

1) $Mf_r$ is large
2) $Mf_r \leq \gamma c/(4\ D)$, where $0 < \gamma < 1$ and $D$ is the maximum human chest displacement magnitude. It can be easily shown that $|\theta_n| \leq \frac{4\pi Mf_r D}{c}$. When $Mf_r \leq \gamma c/(4\ D)$, $|\theta_n| \leq \gamma\pi$.
3) $|P(Mf_r)|$ is large.

Based on these criteria, the integer $M$ is selected as

$$M = \arg \max_{M \leq \gamma c/(4f_r D)} Mf_r |P(Mf_r)|, \tag{19}$$

which avoids the worst-case bias, maximizes SNR, and reduces the CRLB. In this paper, we make heuristic choice of $\gamma = 1/2$ and $D = 7$mm.

## IV. SIMULATION RESULTS

Simulations are conducted to evaluate the estimation performance of the proposed method. A record of real chest respiratory signal obtained by inductance plethysmography available on PhysioNet [50]. Since the record is in unit of Voltage, we linearly scale it to simulate the absolute chest displacement which serves as reference. The transmitted UWB pulse is a 7$^{\text{th}}$-order monocycle with bandwidth scaling factor of 0.3 ns [46]. The pulse repetition frequency, $f_r$, is set to 5 kHz. The nominal distance between the radar and the subject is assumed to be 0.5m. $M$ is selected according to (19), resulting in $M = 1,063,846$ and $Mf_r \approx 5.32$ GHz.

Fig. 7 shows the reference chest displacement waveform and its estimate using the ML estimator (Fig. 7a) and DML estimator (Fig. 7b) at SNR = 6 dB. The latter follows the reference displacement waveform accurately. The RMSE is

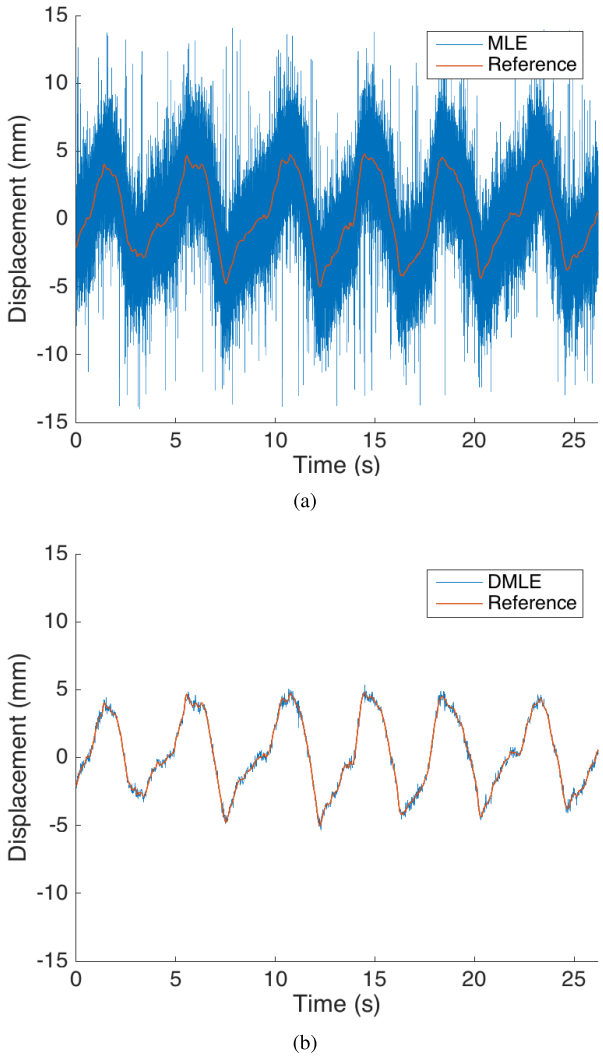


**FIGURE 7.** Displacement estimates with SNR = 6 dB. (a) Maximum likelihood displacement estimates. (b) Displacement estimates after denoising with EMD.

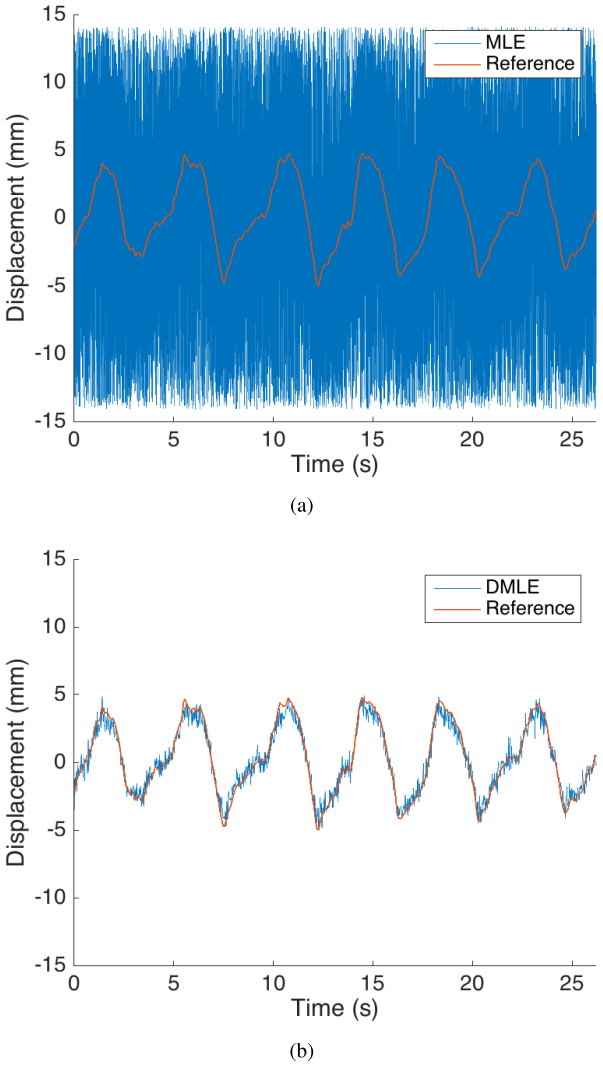


**FIGURE 8.** Displacement estimates with SNR = 0 dB. (a) Maximum likelihood displacement estimates. (b) Displacement estimates after denoising with EMD.

1.77 mm and 0.22 mm for the ML and DML estimates, respectively. Note that the entire displacement waveform containing $N = 131,072$ displacement samples has been estimated at complexity of the N-point DFT.

The estimated chest displacement waveform for SNR = 0 dB is depicted in Fig. 8. Wrapping is observed in the ML waveform. This is explained as follows. The ML displacement estimates are estimated from the phase. In large noise, the phase can be wrapped (see Eq (11)), causing wrapping in the displacement estimate. Although $M$ is selected so that $\theta_n$ is far away from $\pi$ or $-\pi$ as in Section III-D, when the noise is large, $\phi_n$ can deviate away from the truth ($\theta_n$) so much that it wraps. The RMSE is 4.04 mm and 0.55 mm for the ML and DML estimates, respectively.

The performance of the ML and DML estimators for chest displacement due to heart-beating in the absence of breathing is displayed in Fig. 9a and 9b, respectively. This reference displacement is simulated based on the experimental measurements over the apex reported in [7]. In order to simulate the gradual changing of cardiac activity, we read the 10 values from the mean displacement curve at 10 phases along the R-R interval of ECG. In each cardiac cycle, zero-mean Gaussian noise samples are added to these values, and linear interpolation is performed to obtain the displacement samples corresponding to every pulse repetition period. Heart rate variability [51] is also modeled by varying the heart beat period according to a Gaussian random process of mean 0.8 s and standard deviation 0.1 s. As expected, accurate estimation of heartbeat-induced chest displacement needs a much higher SNR due to the much smaller displacement amplitude of the heart-beating compared to that of breathing. The heart beats are discernible in the DML sequence, which is overlaid with the reference displacement in Fig. 9b.

Fig. 10 plots the RMSE of the ML estimator and the CRLB (the square roots of two sides of (18)), and the RMSE of the DML estimator. A sequence of $N = 65,536$ samples

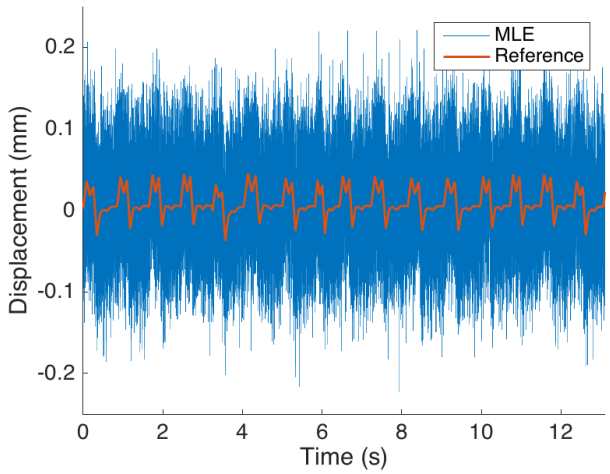


(a)

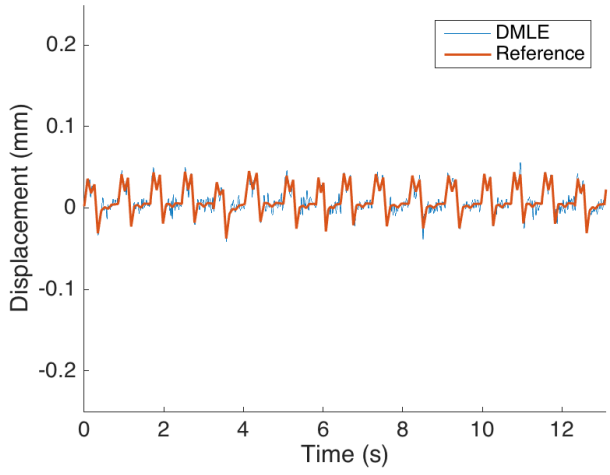


(b)

**FIGURE 9.** Estimates of heartbeating-induced chest displacement during absence of breathing at SNR = 36dB. The mean cardiac cycle is 0.8 s. (a) Maximum likelihood displacement estimates (b) Displacement estimates after denoising with EMD.

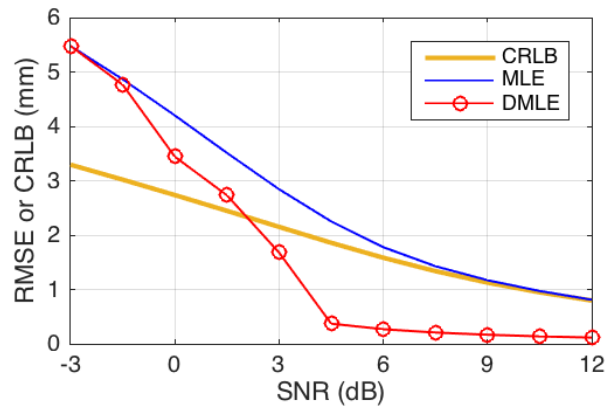


**FIGURE 10.** RMSE of the ML estimator and its associated CRLB, and RMSE of the DML estimator.

equally spaced over the range $[-7, 7]$ mm is used as the chest displacement sequence. This value of $N$ corresponds

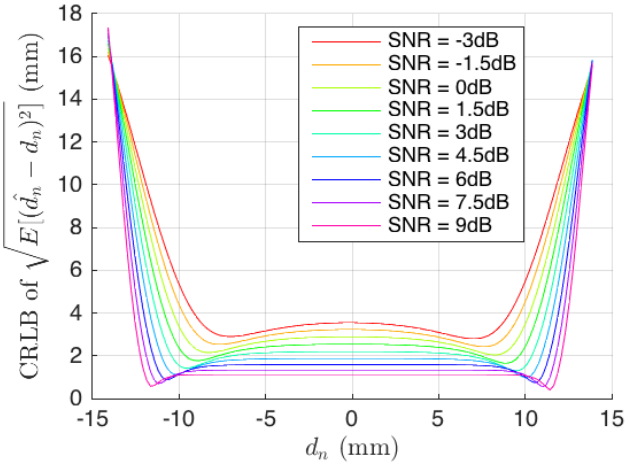


**FIGURE 11.** CRLB of the ML estimator of a displacement sample.

to an observation window of $N/f_r \approx 13$s. The MSE values are averaged over 1000 random noise trials for each SNR value, before being taken square root of. As shown in Fig. 10, the ML estimator approaches the CRLB as SNR increases, and almost achieves the CRLB at SNR $= 12$ dB. It is also shown that denoising improves estimation accuracy for SNR greater than $-3$dB. For SNR $= -3$dB, the DML estimator produces the same estimates with those of the ML estimator, hence the same RMSE value on the plot. The RMSE curve of the DML estimator starts off higher than the CRLB, but strikingly gets below the CRLB at SNR $> 2$ dB. This outperformance over the CRLB is justified, since the CRLB is associated with the ML estimator, not the DML estimator.

The CRLB of the ML estimator for an individual displacement sample is given in Fig. 11. As expected, the displacement CRLB resembles the phase CRLB in Fig. 6, with extreme values near the edges. In the practical range of the human chest displacement of 0 to 7 mm in absolute value, the bound becomes smaller as the displacement magnitude gets larger, although this relationship becomes less dramatic as the SNR increases.

## V. DISCUSSION

In the proposed ML and DML methods, the required captured bandwidth is as small as $f_r$, whose practical values are in the order of kHz, thus there is no need to capture the whole bandwidth of the UWB pulse, which is in the order of GHz. Benefits include significant reduction of sampling rate by several orders of magnitude and of in-band noise. Care must be taken in the hardware implementation to obtain the spectrum portion needed for these methods. One approach is to perform baseband down conversion followed by lowpass filtering, but this approach faces analog issues such as I/Q crosstalk. Another implementation is bandpass filtering followed by passband sampling. Although careful calculation must be taken to derive practical design choices, this approach can avoid most of the analog issues of the down conversion approach.

## VI. CONCLUSION

In this paper, a novel method, DML, that estimates an arbitrary chest displacement waveform from a narrow portion of the IR-UWB received spectrum has been proposed. The method is based on the maximum likelihood (ML) principle followed by denoising. In-depth analysis of bias and CRLB of the ML estimator is also given.

Numerical simulations are performed to evaluate the accuracy of the ML and DML approaches. Realistic simulated chest displacements due to breathing and due to heart beating in the absence of respiration are shown to be accurately reconstructed by the proposed DML method. The ML estimator is observed to approach the CRLB as SNR increases. Strikingly, the DML estimator is shown to outperform this bound for sufficient SNR.

The proposed approach offers several advantages over existing works. Since it uses only a narrow portion of the UWB spectrum, whose bandwidth is on the order of GHz, significant sampling rate reduction can be achieved via passband sampling. In addition, the computational complexity of the proposed method is equal to that of the DFT or that of the denoising method, whichever is larger. When Empirical Mode Decomposition is used for denoising, the complexity is that of the DFT.

A topic of future work is to combine multiple spectral clusters to improve estimation accuracy.

## ACKNOWLEDGMENT

We would like to thank the reviewers for their insightful comments and questions.

## REFERENCES

[1] R. B. Berry *et al.*, "Rules for scoring respiratory events in sleep: Update of the 2007 AASM manual for the scoring of sleep and associated events," *J. Clin. Sleep Med.*, vol. 8, no. 5, pp. 597–619, 2012.

[2] R. B. Berry, R. Brooks, C. E. Gamaldo, S. M. Harding, C. L. Marcus, and B. V. Vaughn, "The AASM manual for the scoring of sleep and associated events," in *Rules, Terminology and Technical Specifications*. Darien, IL, USA: AASM, 2012.

[3] K. Konno and J. Mead, "Measurement of the separate volume changes of rib cage and abdomen during breathing," *J. Appl. Physiol.*, vol. 22, no. 3, pp. 407–422, 1967.

[4] T. Kondo, T. Uhlig, P. Pemberton, and P. D. Sly, "Laser monitoring of chest wall displacement," *Eur. Respirat. J.*, vol. 10, no. 8, pp. 1865–1869, 1997.

[5] W. Massagram, N. Hafner, V. Lubecke, and O. Boric-Lubecke, "Tidal volume measurement through non-contact Doppler radar with DC reconstruction," *IEEE Sensors J.*, vol. 13, no. 9, pp. 3397–3404, Sep. 2013.

[6] M. Zakrzewski, A. Vehkaoja, A. S. Joutsen, K. T. Palovuori, and J. J. Vanhala, "Noncontact respiration monitoring during sleep with microwave Doppler radar," *IEEE Sensors J.*, vol. 15, no. 10, pp. 5683–5693, Oct. 2015.

[7] G. Ramachandran, S. Swarnamani, and M. Singh, "Reconstruction of out-of-plane cardiac displacement patterns as observed on the chest wall during various phases of ECG by capacitance transducer," *IEEE Trans. Biomed. Eng.*, vol. 38, no. 4, pp. 383–385, Apr. 1991.

[8] R. Vas, C. R. Joyner, D. E. Pittman, and T. C. Gay, "The displacement cardiograph," *IEEE Trans. Biomed. Eng.*, vol. BME-23, no. 1, pp. 49–54, Jan. 1976.

[9] M. Okada, T. Nakajima, N. Eizuka, Y. Saitoh, and M. Yakata, "Isochronal map of chest wall vibration with cardiokymography," *Comput. Methods Programs Biomed.*, vol. 26, no. 2, pp. 105–113, 1988.

[10] M. Norgia and S. Donati, "A displacement-measuring instrument utilizing self-mixing interferometry," *IEEE Trans. Instrum. Meas.*, vol. 52, no. 6, pp. 1765–1770, Dec. 2003.

[11] I. Milesi, M. Norgia, P. P. Pompilio, C. Svelto, and R. L. Dellacà, "Measurement of local chest wall displacement by a custom self-mixing laser interferometer," *IEEE Trans. Instrum. Meas.*, vol. 60, no. 8, pp. 2894–2901, Aug. 2011.

[12] A. Periasamy and M. Singh, "Reconstruction of cardiac displacement patterns on the chest wall by laser speckle interferometry," *IEEE Trans. Med. Imag.*, vol. MI-4, no. 1, pp. 52–57, Mar. 1985.

[13] G. Ramachandran and M. Singh, "Three-dimensional reconstruction of cardiac displacement patterns on the chest wall during the P, QRS and T-segments of the ECG by laser speckle inteferometry," *Med. Biol. Eng. Comput.*, vol. 27, no. 5, pp. 525–530, Sep. 1989.

[14] M. Singh and G. Ramachandran, "Reconstruction of sequential cardiac in-plane displacement patterns on the chest wall by laser speckle interferometry," *IEEE Trans. Biomed. Eng.*, vol. 38, no. 5, pp. 483–489, May 1991.

[15] X. Gao and O. Boric-Lubecke, "Radius correction technique for Doppler radar noncontact periodic displacement measurement," *IEEE Trans. Microw. Theory Techn.*, vol. 65, no. 2, pp. 621–631, Feb. 2017.

[16] B.-K. Park, O. Boric-Lubecke, and V. M. Lubecke, "Arctangent demodulation with DC offset compensation in quadrature Doppler radar receiver systems," *IEEE Trans. Microw. Theory Techn.*, vol. 55, no. 5, pp. 1073–1079, May 2007.

[17] X. Gao, A. Singh, E. Yavari, V. Lubecke, and O. Boric-Lubecke, "Non-contact displacement estimation using Doppler radar," in *Proc. Annu. Int. Conf. IEEE Eng. Med. Biol. Soc.*, Aug./Sep. 2012, pp. 1602–1605.

[18] W. Hu, Z. Zhao, Y. Wang, H. Zhang, and F. Lin, "Noncontact accurate measurement of cardiopulmonary activity using a compact quadrature Doppler radar sensor," *IEEE Trans. Biomed. Eng.*, vol. 61, no. 3, pp. 725–735, Mar. 2014.

[19] Y. S. Lee, P. N. Pathirana, C. L. Steinfort, and T. Caelli, "Monitoring and analysis of respiratory patterns using microwave Doppler radar," *IEEE J. Trans. Eng. Health Med.*, vol. 2, pp. 1–12, 2014.

[20] Z. Wu and N. E. Huang, "Ensemble empirical mode decomposition: A noise-assisted data analysis method," *Adv. Adapt. Data Anal.*, vol. 1, no. 1, pp. 1–41, 2008.

[21] S. Guan, J. A. Rice, C. Li, and C. Gu, "Automated DC offset calibration strategy for structural health monitoring based on portable CW radar sensor," *IEEE Trans. Instrum. Meas.*, vol. 63, no. 12, pp. 3111–3118, Dec. 2014.

[22] M. Zakrzewski, H. Raittinen, and J. Vanhala, "Comparison of center estimation algorithms for heart and respiration monitoring with microwave Doppler radar," *IEEE Sensors J.*, vol. 12, no. 3, pp. 627–634, Mar. 2012.

[23] "Revision of part 15 of the commission rules regarding Ultrawideband transmission systems, first report and order," Federal Commun. Commission, Washington, DC, USA, Tech. Rep. ET Docket 98–153, 2002.

[24] E. M. Staderini, "UWB radars in medicine," *IEEE Aerosp. Electron. Syst. Mag.*, vol. 17, no. 1, pp. 13–18, Jan. 2002.

[25] J. C. Y. Lai *et al.*, "Wireless sensing of human respiratory parameters by low-power ultrawideband impulse radio radar," *IEEE Trans. Instrum. Meas.*, vol. 60, no. 3, pp. 928–938, Mar. 2011.

[26] Y. Nijsure *et al.*, "An impulse radio ultrawideband system for contactless noninvasive respiratory monitoring," *IEEE Trans. Biomed. Eng.*, vol. 60, no. 6, pp. 1509–1517, Jun. 2013.

[27] G. Ossberger, T. Buchegger, E. Schimback, A. Stelzer, and R. Weigel, "Non-invasive respiratory movement detection and monitoring of hidden humans using ultra wideband pulse radar," in *Proc. IEEE Int. Workshop Ultra Wideband Syst., Joint Conf. Ultrawideband Syst. Technol. Joint UWBST IWUWBS*, May 2004, pp. 395–399.

[28] M. Baldi, F. Chiaraluce, B. Zanaj, and M. Moretti, "Analysis and simulation of algorithms for vital signs detection using UWB radars," in *Proc. IEEE Int. Conf. Ultra-Wideband (ICUWB)*, Sep. 2011, pp. 341–345.

[29] B. Schleicher, I. Nasr, A. Trasser, and H. Schumacher, "IR-UWB radar demonstrator for ultra-fine movement detection and vital-sign monitoring," *IEEE Trans. Microw. Theory Techn.*, vol. 61, no. 5, pp. 2076–2085, May 2013.

[30] M. Y. W. Chia, S. W. Leong, C. K. Sim, and K. M. Chan, "Through-wall UWB radar operating within FCC's mask for sensing heart beat and breathing rate," in *Proc. IEEE EURAD*, Oct. 2005, pp. 267–270.

[31] M. Leib *et al.*, "A compact ultra-wideband radar for medical applications," *Frequenz*, vol. 63, nos. 1–2, p. 2, 2009.

[32] M. Leib, W. Menzel, B. Schleicher, and H. Schumacher, "Vital signs monitoring with a UWB radar based on a correlation receiver," in *Proc. IEEE EuCAP*, Apr. 2010, pp. 1–5.

[33] M. Muller and G. I. Abib, "Ultra wideband RADAR system for human chest displacement," in *Proc. IEEE NEWCAS*, Jun. 2015, pp. 1–4.

[34] M. Muragaki *et al.*, "Noncontact respiration monitoring of multiple closely positioned patients using ultra-wideband array radar with adaptive beamforming technique," in *Proc. IEEE ICASSP*, Mar. 2017, pp. 1118–1122.
[35] F. Sana, T. Ballal, T. Y. Al-Naffouri, and I. Hoteit, "Low-complexity wireless monitoring of respiratory movements using ultra-wideband impulse response estimation," *Biomed. Signal Process. Control*, vol. 10, pp. 192–200, Mar. 2014.
[36] J. Li and R. Wu, "An efficient algorithm for time delay estimation," *IEEE Trans. Signal Process.*, vol. 46, no. 8, pp. 2231–2235, Aug. 1998.
[37] V. Nguyen and M. A. Weitnauer, "Theoretical spectral analysis of the IR-UWB radar chest reflection with arbitrary periodic breathing- and heart-induced displacements," *Prog. Electromagn. Res. B*, vol. 71, pp. 119–135, Nov. 2016.
[38] J. Zhang, R. A. Kennedy, and T. D. Abhayapala, "Cramer–Rao lower bounds for the time delay estimation of UWB signals," in *Proc. IEEE Int. Conf. Commun.*, vol. 6. Jun. 2004, pp. 3424–3428.
[39] S. Gezici, "Theoretical limits for estimation of periodic movements in pulse-based UWB systems," *IEEE J. Sel. Topics Signal Process.*, vol. 1, no. 3, pp. 405–417, Oct. 2007.
[40] G. Yuan, N. A. Drost, and R. A. McIvor, "Respiratory rate and breathing pattern," *McMaster Univ. Med. J.*, vol. 10, no. 1, pp. 23–25, 2013.
[41] N. E. Huang *et al.*, "The empirical mode decomposition and the Hilbert spectrum for nonlinear and non-stationary time series analysis," *Proc. Roy. Soc. London Ser. A, Math., Phys. Eng. Sci.*, vol. 454, no. 1971, pp. 903–995, Mar. 1998.
[42] A. Hyvärinen, J. Karhunen, and E. Oja, *Independent Component Analysis*, vol. 46. New York, NY, USA: Wiley, 2004.
[43] G. L. Stüber, *Principles of Mobile Communication*. New York, NY, USA: Springer, 2011.
[44] Y.-H. Wang, C.-H. Yeh, H.-W. V. Young, K. Hu, and M.-T. Lo, "On the computational complexity of the empirical mode decomposition algorithm," *Phys. A, Statist. Mech. Appl.*, vol. 400, pp. 159–167, Apr. 2014.
[45] D. Feng, M. Q. Feng, E. Ozer, and Y. Fukuda, "A vision-based sensor for noncontact structural displacement measurement," *Sensors*, vol. 15, no. 7, pp. 16557–16575, 2015.
[46] B. Hu and N. C. Beaulieu, "Pulse shapes for ultrawideband communication systems," *IEEE Trans. Wireless Commun.*, vol. 4, no. 4, pp. 1789–1797, Jul. 2005.
[47] D. C. Rife and R. R. Boorstyn, "Single tone parameter estimation from discrete-time observations," *IEEE Trans. Inf. Theory*, vol. 20, no. 5, pp. 591–598, Sep. 1974.
[48] P. Dharmawansa, N. Rajatheva, and C. Tellambura, "Envelope and phase distribution of two correlated Gaussian variables," *IEEE Trans. Commun.*, vol. 57, no. 4, pp. 915–921, Apr. 2009.
[49] Don H. Johnson. (2013). *Statistical Signal Processing*. [Online]. Available: https://www.ece.rice.edu/~dhj/courses/elec531/notes.pdf
[50] A. L. Goldberger *et al.*, "PhysioBank, PhysioToolkit, and PhysioNet: Components of a new research resource for complex physiologic signals," *Circulation*, vol. 101, no. 23, pp. e215–e220, Jun. 2000. [Online]. Available: http://circ.ahajournals.org/content/101/23/e215.full, doi: 10.1161/01.CIR.101.23.e215.
[51] M. Malik, "Heart rate variability," *Ann. Noninvasive Electrocardiol.*, vol. 1, no. 2, pp. 151–181, 1996.

**VAN NGUYEN** received the M.S. and Ph.D. degrees in electrical and computer engineering from the Georgia Institute of Technology in 2011 and 2016, respectively, with a focus on statistical signal processing and algorithm development with impulse radio ultra wideband (IR-UWB) radar for noncontact physiological sensing. She was a Research Assistant, and a Teaching Assistant for numerous undergraduate and graduate classes. She is currently a Senior Audio CODEC Engineer at Qualcomm, San Diego, CA, USA. She received the Vietnam Education Foundation Fellowship from 2009 to 2011.

**MARY ANN WEITNAUER** (M'83–SM'03) was a Visiting Professor at Aalborg University, Aalborg, Denmark, from 2006 to 2008 and at Idaho National Labs in 2010. She held the Georgia Tech ADVANCE Professorship with the College of Engineering from 2006 to 2012. She is currently a Professor and a Senior Associate Chair with the School of Electrical and Computer Engineering, Georgia Tech, where she has been a Faculty Member since 1989. Her research is focused on the lower three layers of MIMO wireless networks that have virtual or distributed antenna arrays. Many results are demonstrated on a 20-node network of software-defined radios (SDRs) in practical environments and topologies. She has authored or co-authored over 200 refereed journal and conference papers. She received four best paper awards in conferences. She was an Associate Editor of the IEEE TRANSACTIONS ON MOBILE COMPUTING from 2009 to 2012.